# Physicochemical characteristics that affect carbon dot safety: Lessons from a comprehensive study on a nanoparticle library

Jiahui Fan, Mickaël Claudel, Carole Ronzani, Yasmin Arezki, Luc Lebeau, Françoise Pons

*Graphical Abstract (for review)

## Dose-dependent cytotoxicity

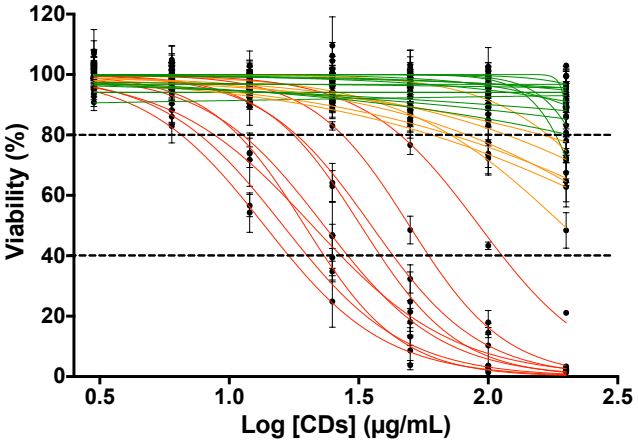


## Synthesis of a carbon dot library

Carbon source

Passivation Agent

Reagent ratio

Carbonization procedure
+/-
Post-functionalization

35 carbon dots

## Cytotoxicity and size

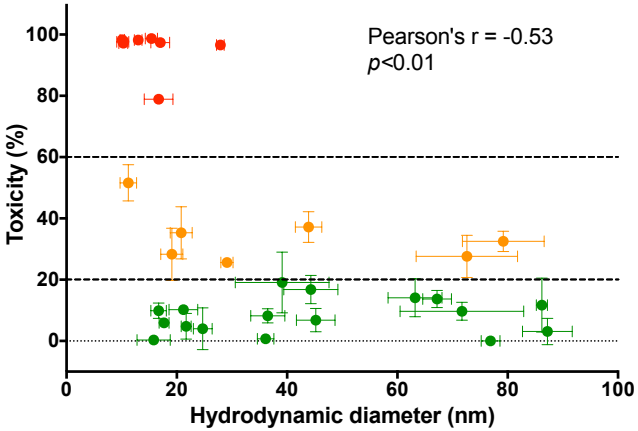


## Cytotoxicity and charge

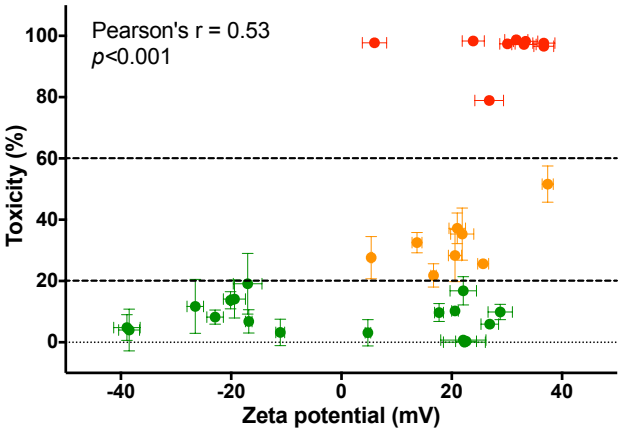


## Cytotoxicity and composition

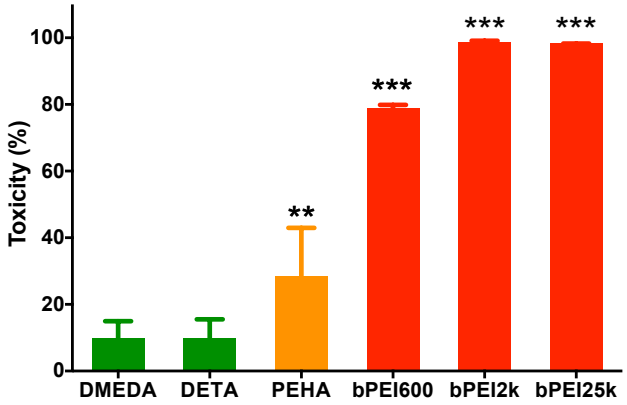

# Physicochemical characteristics that affect carbon dot safety: lessons from a comprehensive study on a nanoparticle library

Jiahui Fan, Mickaël Claudel, Carole Ronzani, Yasmin Arezki, Luc Lebeau, Françoise Pons*

Laboratoire de Conception et Application de Molécules Bioactives, UMR 7199,
CNRS-Université de Strasbourg, Faculté de Pharmacie, Illkirch, France

* Corresponding author

Full postal address: UMR 7199, Faculté de Pharmacie, 74 route du Rhin, 67400 Illkirch, France
E-mail: pons@unistra.fr

Phone: (+33) 3 68 85 42 03

Fax : (+33) 3 68 85 43 06

**Abstract**

Carbon dots (CDs) are emerging nanomaterial in medicine and pharmacy. To explore the impact of physicochemical characteristics on their safety, we synthesized a library of 35 CDs exhibiting different size, charge, chemical composition and surface coating, using various starting materials (carbon source and passivation reagent) and carbonization procedures. The 35 CDs triggered different levels of viability loss when incubated with human macrophages at 3-200 µg/mL for 24 h. The smaller NPs (10-20 nm) were more toxic that larger ones (40-100 nm), whereas NPs that aggregated in culture medium were more toxic than dispersed ones. A positive correlation was found between CD charge or nitrogen content and toxicity. Furthermore, a greater toxicity was observed for CDs prepared from high molecular weight polyamines, suggesting a role of the CD global density of positive charges, rather than the charge at the CD surface, in the CD toxicity. At last, PEG decoration decreased the toxicity of cationic NPs. In conclusion, the size, aggregation in culture medium, charge, nitrogen content, nature of the passivation agent and synthesis procedure were found to influence CD toxicity, making it difficult to predict CD safety from a single characteristic.

**Keywords**

nanoparticle ; carbon dot ; toxicity ; size ; charge ; surface chemistry.

**Abbrevations**

bPEI : branched polyethyleneimine ; CD : carbon dot ; DLS : dynamic light scattering ; DMEDA : *N,N*-dimethylethylene diamine ; DETA : diethylenetriamine ; EA : ethanolamine ; EDC : *N*-(3-dimethylaminopropyl)-*N'*-ethylcarbodiimide hydrochloride ; lPEI : linear polyethyleneimine ; mPEG : poly(ethylene glycol) monomethyl ether ; MW : microwave-assisted pyrolysis under atmospheric pressure ; MW-ST : microwave-assisted pyrolysis under solvothermal conditions ; MWCO : molecular weight cut-off ; NP : nanoparticle ; PEHA : pentaethylenehexamine ; PES : polyethersulfone ; PMA : phorbolmyristate acetate ; Post-F : post-functionnalization ; Pyro : conventional pyrolysis under atmospheric pressure ; TEM : transmission electron microscopy ; ST : solvothermal treatment

## 1. Introduction

Carbon dots (CDs) are small-sized (a few nm) spherical carbonaceous nanomaterials that exhibit water dispersibility, chemical stability, intrinsic photoluminescence properties and photostability (Himaja et al., 2015; Kwon et al., 2014; Sachdev et al., 2014; Tian et al., 2014). This last member of the carbon nanoparticle (NP) family to be discovered (Xu et al., 2004) is easily produced from inexpensive starting materials by either top-down or bottom-up synthesis methods. In the top-down approaches, CDs are produced by breaking down large carbon structures, such as carbon powders, carbon nanotubes, graphite columns or graphene by electrochemical synthesis, chemical oxidation or solvothermal synthesis. In the bottom-up approaches, they are built by the pyrolysis of organic matter (e.g., citric acid, glucose, phenylenediamine, urea, fruit juice…) in the presence of catalysts and/or passivating agents, using various activation processes (hydrothermal methods, microwave irradiation…). By varing the nature of the carbon source, catalyst and passivation agent, and the synthesis process, the core and surface characteristics of CDs can be tuned to endow specific physicochemical, optical, and biological properties (Gong et al., 2019; Huang et al., 2019; Xia et al., 2018; Xie et al., 2019).

Due to their unique properties, CDs have potential applications in various fields, including medicine and pharmacy. Fluorescent CDs with superior photostability are currently developed for optical imaging as an alternative to metal-based semiconductor quantum dots (Edison et al., 2016 ; Qian et al., 2014; Ray et al., 2009; Stefanakis et al., 2014; Yang et al., 2009). CDs are also emerging as versatile nanoplatforms for the delivery of therapeutic agents such as paclitaxel or doxorubicin (Gomez et al., 2018; Yuan et al., 2017; Zhang et al., 2017). When surface-passivated with nitrogen-containing reagents, CDs may be cationic and may form complexes with nucleic acids through electrostatic interactions. They may thus be used as gene delivery systems as demonstrated both *in vitro* (Claudel et al., 2019; Dou et al., 2015; Hu et al., 2014; Liu et al., 2012; Pierrat et al., 2015; Wang et al., 2014; Yang et al., 2017) *and in vivo* (Kim et al., 2017; Pierrat et al., 2015). According to recent publications, CDs are also good candidates for theranostic applications bringing new hopes for the care of diseases such as cancer (Hassan et al., 2018; Hola et al., 2014; Wu et al., 2016).

Because of their specific properties at the nanoscale, engineered nanomaterials raise safety concerns which appear to be linked to their physicochemical characteristics, including

composition, size, charge and surface chemistry (Gatoo et al., 2014; Luyts et al., 2013; Nel et al., 2006). Although carbon is not considered as a toxic element, some carbon-based nanomaterials such as pristine carbon nanotubes or $C_{60}$-fullerenes have raised some concerns (Li et al., 2013 ; Ronzani et al., 2012 ; Salieri et al., 2017). Thus, developing CDs for biomedical applications requires assessing not only their efficacy, but also their safety. In the literature, CDs have been reported so far to cause little if any toxicity, and are therefore considered as biocompatible (Blas-Garcia et al., 2016; Edison et al., 2016; Emam et al., 2017; Lategan et al., 2018; Li et al., 2015; Qian et al., 2014; Ray et al., 2009; Wang et al., 2013; Yang et al., 2009). However most studies were carried out on pristine CDs or on CDs that were surface-passivated with poly(ethylene glycol) (PEG), which is a biocompatible polymer used to prevent NP opsonisation and recognition by the immune system. These studies may thus not properly reflect the safety of CDs towards living cells. In agreement with this hypothesis, CDs produced from branched polyethyleneimine 25 kDa (bPEI25k) or obtained from candle soot and subsequently passivated with PEI so they display a net positive charge, were reported to exhibit some cytotoxicity towards cultured cells from various tissue origins (Liu et al., 2012; Pierrat et al., 2015; Ronzani et al., 2018). In contrast, negatively charged CDs were found to have limited toxicity (cell viability loss was less than 20 % at concentration higher than 250 µg/mL) on murine macrophages (Lategan et al., 2018). Therefore, physicochemical characteristics of CDs, among which surface chemistry and charge, may impact their safety. The carbon source used to produce CDs could also play a role, as suggested in a very recent study (Cailotto et al., 2018). As well, the very small size of the NPs might favor their biological reactivity, and thus their toxicological effects. At last, the mode of synthesis of CDs is another possible influencing factor as it may lead to different NPs from the same starting materials (Claudel et al., 2019). However, all these factors remain so far poorly explored.

In the present study, we synthesized a library of 35 CDs exhibiting various size, charge and surface chemistry by the pyrolysis of citric acid (or salts thereof), D-mannitol or PEG as a source of carbon, in the presence of diverse passivation agents (ethanolamine (EA), *N,N*-dimethylethylenediamine (DMEDA), diethylenetriamine (DETA), pentaethylenehexamine (PEHA), and linear or branched poly(ethyleneimine) (PEI) of various molecular weight) and catalysts (HCl, $H_3PO_4$, $H_2SO_4$…), and using different bottom-up synthesis methods and carbonization procedures (solvothermal treatment (ST), conventional pyrolysis under atmospheric pressure (Pyro), or microwave-assisted pyrolysis under atmospheric pressure (MW) or under solvothermal condition (MW-ST)) followed in some instance by further chemical transformation referred to as post-functionalization (Post-F) (Figure 1). The size, charge, and

elemental composition of these nanomaterials were determined, as well as their toxicity towards THP-1-derived macrophages. Then, relationships between physicochemical characteristics of CDs and their safety were analyzed.

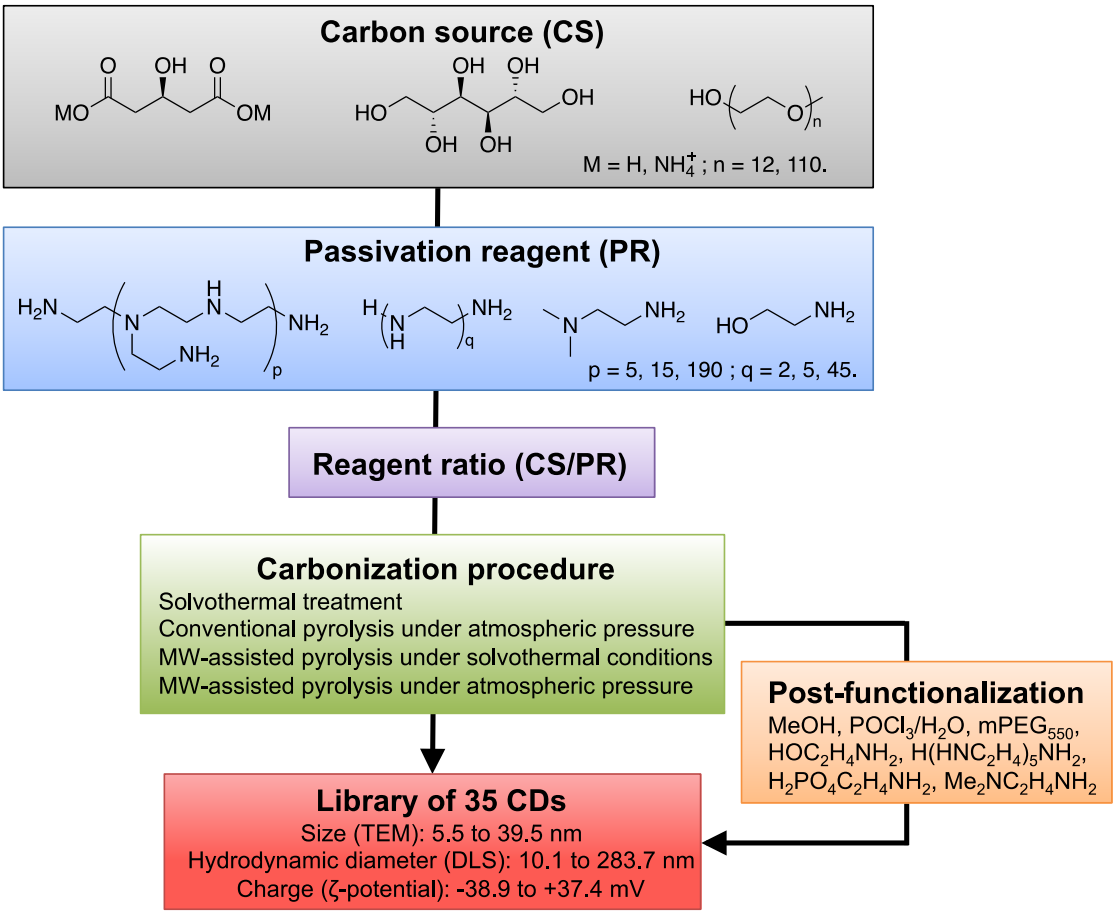


**Figure 1:** General flow chart for the synthesis of the 35 CDs investigated in this work.

## 2. Materials and methods

### *2.1. Preparation of CDs*

Solvothermal preparation (ST)

Citric acid (2.5 g), bPEI600 (5.0 g), and $H_2O$ (50 mL) were mixed under vigorous stirring to form a homogeneous solution that was transferred into a reaction vessel fitted with a reflux condenser, and heated for 24 h at 100 °C. When cooled down to room temperature, the resulting colored solution was transferred into a dialysis bag (Spectra/Por 3, MWCO 1,000 Da) and was equilibrated for 12 h against 1 L HCl 0.1 N (dialysate was replaced at 1, 3, 7 h), and then against ultra-pure water for an additional 12 h-period. Finally the brown-yellow solution was filtered through a 0.22 µm PES membrane (Millex) and freeze-dried at –50 °C for 24-36 h to yield a hygroscopic powdered yellow material (**CD25**, 532 mg). **CD26** (663 mg) and **CD32** (2.85 g) were obtained similarly, by reacting citric acid (1.0 g) with bPEI600 (5.0 g), and citric acid (5.0 g) with bPEI25k (2.5 g), respectively.

Pyrolysis under conventional heating and solvent-free conditions (Pyro)

Citric acid (6.0 g) and D-mannitol (17.0 g) were mixed in a 50 mL borosilicate reaction flask without solvent and heated at 150 °C for 30 min under atmospheric pressure. During this first heating step, volatile was integrally driven out of the reaction vessel. Then, the temperature was raised to and maintained at 230 °C for an additional period of 30 min. The resulting reaction mixture was cooled down to room temperature, dissolved in water and dialyzed (Spectra/Por 3, MWCO 100-500 Da) for 24 h. The resulting brown solution was filtered through a 0.22 µm PES membrane and freeze-dried to yield a hygroscopic powdered black material (**CD4**, 2.54 g). **CD10** (1.65 g), **CD12** (2.40 g), **CD16** (3.02 g), **CD18** (5.63 g), **CD23** (1.79 g), **CD24** (3.62 g), **CD29** (0.22 g), **CD30** (2.13 g) and **CD35** (2.76 g) were prepared similarly replacing D-mannitol by EA (6.0 g), DMEDA hydrochloride (11.3 g), DETA (23.0 g), PEHA (21.7 g), bPEI600 (12.0 g), bPEI600 (24.0 g), lPEI2k (3.0 g), lPEI2k (24.0 g), bPEI2k (24.0 g), and bPEI25k (24.0 g), respectively. **CD29**, **CD30** and **CD35** were dialyzed on a membrane with MWCO 1,000 Da. The same protocol, was carried out to produce **CD14** (reagents: 0.5 g citric acid, 4.3 g mPEG550 and 1.0 g DMEDA; dialysis: MWCO 1,000 Da; yield: 0.64 g), **CD19** (reagents: 0.5 g citric acid, 4.3 g mPEG550, and 1.8 g PEHA; dialysis: MWCO 1,000 Da; yield: 0.21 g), and **CD20** (reagents: 0.5 g citric acid, 4.3 g mPEG5000 and 1.8 g PEHA; dialysis: MWCO 12,000 Da; yield: 0.49 g).

Alternatively, citric acid (2.0 g) and DMEDA (8.0 g) were vigourously mixed in HCl 12 N (7.8 mL) and heated at 100 °C, volatiles being continuously driven out of the reaction vessel. After 45 min, the temperature was increased to 230 °C and the reaction mixture was stirred for an additional 45-min period at this temperature. The mixture was then cooled down to room temperature, dissolved in water, dialyzed (MWCO 1,000 Da), and freeze-dried to yield a light brown hygroscopic solid (**CD13**, 0.05 g).

Citric acid (6.3 g) and DETA (10.5 g) were strirred at 160 °C for 3 h, volatiles being continuously driven out of the reaction vessel. The resulting mixture was cooled down to room temperature, dissolved in water (20 mL), dialyzed (MWCO 100-500 Da), and freeze-dried to yield a dark brown hygroscopic solid (**CD15**, 1.27 g).

Preparations under microwave irradiation (MW and MW-ST)

For MW preparation, ammonium citrate (5.0 g) and $KH_2PO_4$ (1.0 g) in ultrapure water (10 mL) were mixed in an Erlenmeyer flask to form a homogeneous solution that was heated in a domestic microwave oven at 700 W for 120 s (*i.e.*, under atmospheric pressure). The crude residue was stirred in refluxing EtOH (50 mL) for 4 h and cooled down at 4°C overnight. The supernatant was filtered through a 0.22 µm PES membrane and the solvent was removed under reduced pressure to yield **CD1** (0.70 g). To exchange ammonium counter ion with $Na^+$, **CD1** (0.50 g) was dissolved in ultra pure water and pH was adjusted to 12 (NaOH 1N) before lyophilisation, yielding **CD2** (0.67 g).

Alternatively, citric acid (500 mg), bPEI25k (125 mg), and HCl 0.1 N (5 mL) were mixed in an Erlenmeyer flask under vigorous stirring to form a homogeneous solution that was heated in a domestic microwave oven at 620 W for 170 s. The residue was dissolved in HCl 0.1 N, centrifuged (10,000 rpm, 5 min), and supernatant was loaded in a dialysis bag (MWCO 3,500 Da) for extensive dialysis against HCl 0.1 N (24 h) and ultra pure water (24 h). Lyophilization yielded **CD9** (92 mg). **CD21** (reagents: 250 mg citric acid, 500 mg bPEI600, 5 mL HCl 0.1 N; dialysis: MWCO 1,000 Da; yield: 116 mg), **CD22** (reagents: 125 mg citric acid, 500 mg bPEI600, 5 mL HCl 0.1 N; dialysis: MWCO 100-500 Da; yield: 275 mg), **CD31** (reagents: 500 mg citric acid, 250 mg bPEI25k, 5 mL HCl 1 N; dialysis: MWCO 3,500 Da; yield: 223 mg), **CD33** (reagents: 250 mg citric acid, 500 mg bPEI25k, 5 mL HCl 0.1 N; dialysis: MWCO 3,500 Da; yield: 60 mg), and **CD34** (reagents: 125 mg citric acid, 500 mg bPEI25k, 5 mL HCl 1 N; dialysis: MWCO 3,500 Da; yield: 31 mg) were obtained similarly.

In another protocol, microwave irradiation was carried out under solvothermal conditions

(MW-ST). Citric acid (1.0 g), bPEI600 (2.0 g), and water (10 mL) were introduced into a tightly sealed borosilicate glass vial and heated at 100 °C, for 30 min, using an Anton Paar Monowave 500 microwave reactor. The crude residue was purified by dialysis (MWCO 1,000 Da) and yielded a yellow powdered material upon freeze-drying (**CD27**, 0.24 g). **CD28** (reagents: 1.0 g citric acid, 4.0 g; bPEI600, 10 mL $H_2O$; dialysis: MWCO 1,000 Da; yield: 0.22 g) was obtained similarly.

CD Post-functionalization (Post-F)

**CD2** (0.50 g) was treated with thionyl chloride (50 µL) in refluxing methanol (10 mL) for 48 h. Evaporation of the volatiles yielded a greenish hygroscopic material (**CD3**, 0.46 g).

**CD4** (0.50 g) was stirred in phosphorus oxychloride (10 mL) for 48 h at room temperature. Then volatiles were removed under reduced pressure, and the crude residue was dissolved in pure water. It was decomposed by slow addition of $NaHCO_3$ until pH reached neutrality. The resulting suspension was centrifuged (10,000 rpm, 5 min) and the supernatant was dialyzed (MWCO 100-500 Da) to yield a brown hygroscopic powdered material (**CD5**, 0.16 g) upon freeze-drying.

**CD2** (0.30 g) was refluxed in $SOCl_2$ (5 mL) for 3 h. Volatiles were removed under reduced pressure, mPEG550 (3.00 g) was added, and the resulting suspension was heated at 130 °C for 72 h. The crude reaction mixture was dialyzed (MWCO 1,000 Da) to yield a light brown viscous oil upon freeze-drying (**CD6**, 0.67 g). **CD8** (0.10 g), **CD11** (0.20 g), and **CD17** (0.21 g) were obtained similarly, unless the reaction was conducted in toluene and mPEG550 was replaced by EA (4.80 g), DMEDA (1.50 g), or PEHA (1.50 g), respectively. Solvent was removed under reduced pressure and replaced by water before dialysis (MWCO 100-500 Da).

Alternatively, **CD2** (0.30 g) and EDC (0.30 g) were dissolved in $H_2O$ (3 mL), and pH of the solution was set to neutrality before phosphoethanolamine (0.30 g) was added. The reaction mixture was stirred at room temperature for 96 h. Then, 0.1 M $NaH_2PO_4$ (10 mL) was added, and the crude mixture was dialyzed (MWCO 100-500 Da) to yield a slightly yellow hygroscopic powdered material (**CD7**, 0.12 g) upon freeze-drying.

*2.2. Characterization of CDs*

Size of CDs was determined by transmission electron microscopy (TEM) using a bench top

transmission electron microscope operating at 5 kV (LVEM5, Cordouan Technologies, Pessac, France). Carbon-coated grids (Cu-300HD, Pacific Grid Tech, San Francisco, USA) were glow discharged at 90 V and 2 mA for 15 s before deposition of the CD samples (0.5 µL, 1 mg/mL in 1.5 mM NaCl pH 7.4). The grids were allowed to dry at room temperature for at least 2 h before observation. Average size of the particles was determined by image analysis using the ImageJ software (v 1.50i, NIH, USA), from a set of 300-1000 particles.

The hydrodynamic diameter and zeta potential (ζ) of CDs were measured by dynamic light scattering (DLS) using a Zetasizer NanoZS apparatus (Malvern Instruments, Paris, France). Measurements were performed in triplicate on fresh samples prepared at 1 mg/mL in 1.5 mM NaCl pH 7.4, and at 25 °C. Data were analyzed using the multimodal number distribution software supplied with the instrument and expressed as mean (± SD).

DLS measurements were also used to determine the aggregation state of CDs in culture medium. CD dispersion were prepared at 1 mg/mL in complete RPMI-1640 without sonication, and measurements were performed in triplicate at 25 °C (see below), extemporaneously.

The elemental composition of CDs was determined by analysis on a Vario EL III instrument (Elementar, Langenselbold, Germany) and expressed as carbon (C), hydrogen (H), and nitrogen (N) mass fractions (%).

### *2.3. Cell culture*

Non activated THP-1 cells (TIB-202™, ATCC) were grown in culture flasks at 37 °C in a 5 % $CO_2$ humidified chamber using RPMI-1640 culture medium containing 2 mM L-glutamine, 0.05 mM 2-mercaptoethanol, 100 UI/mL penicillin, 100 µg/mL streptomycin and 10 % heat inactivated foetal bovine serum (all reagents from GIBCO). When the culture reached 0.8-1.0x$10^6$ cells/mL, cells were centrifuged and were resuspended in culture medium at a 2.5x$10^5$ cells/mL density to establish subcultures or were seeded in culture plates for differentiation into macrophages and assessment of CD toxicity.

### *2.4. Assessment of CD toxicity*

Toxicity of CDs was assessed by measuring changes in cell viability using the MTT assay. Cells were seeded into 96-well culture plates at a density of $10^5$ cells/well, and differentiated into macrophages overnight by adding 10 ng/mL phorbolmyristate acetate (PMA, Sigma-Aldrich) to

the culture medium. The following day, cells were incubated with increasing concentrations of CDs (3-200 µg/mL) for 24 h. Then, cells were carefully washed with PBS before addition of 100 µL MTT (1.0 mg/mL in complete culture medium). After a 1-h incubation period, culture medium was removed and cells were lysed with DMSO. Absorbance of the resulting samples was read at 570 nm with a correction at 690 nm using a Multiskan FC reader (Thermo Scientific). Cell viability was expressed as the percentage of the absorbance of treated cells relative to the absorbance of the non-exposed control cells.

*2.5. Presentation and statistical analysis of the data*

Data were plotted as concentration-response curves, scatter plots or bar charts and were analyzed with the GraphPad Prism 6.0 software. Concentration-response curves were obtained after logarithmic transformation of the data and fit with the Hill equation. Then, the Hill equation was used to calculate the half maximal effective concentration (EC50) or effective concentration triggering 20% viability loss (EC20), when possible. Scatter plot representations were used to analyse relationships between physicochemical characteristics of CDs (size, charge, nitrogen, carbon and hydrogen content) and their cytotoxicity. The Pearson's correlation test was applied to evaluate the correlation and calculate the Perason's r. In the bar chart representations, statistical differences between groups were determined by one or two-way ANOVA followed by the Dunnett's test. Data were considered as significantly different when $p$ value was less than 0.05.

## 3. Results and Discussion

### *3.1. Synthesis of CDs*

The bottom-up approach to produce CDs through a one-pot carbonization processing of simple organic compounds or more complex organic matter (food stuff, agricultural waste, hair, *Bombyx mori* silk…) has been especially popular over the last decade (Himaja et al., 2015; Li et al., 2012; Zuo et al., 2016). This is likely due to the easy implementation of the synthetic protocol, such as simple heating of precursors at high temperature (180–250 °C) for a few hours. Depending on the starting material(s) and combustion/thermal treatment, CDs may display a wide range of physical properties (size, charge, surface chemistry, optical properties). In this work, a collection of 35 CDs were synthesized using varying protocols and starting materials in order to generate NP diversity and allow investigation on the impact of the physicochemical characteristics of these nanomaterials on their safety. The CDs were thus produced from various carbon sources (citric acid and salts thereof, D-mannitol and mPEG) and passivation reagents (EA, DMEDA, DETA, PEHA, bPEI600, bPEI2k, lPEI2k, and bPEI25k) in different ratios (1:1.4 to 4:1) that were submitted to different thermal treatments (solvothermal synthesis under conventional heating (ST) or microwave irradiation (MW-ST), pyrolysis under conventional heating and solvent-free conditions (Pyro), microwave-assisted pyrolysis (MW)), under normal or high pressure (Table 1). Some of these CDs were further modified through surface grafting with various functional groups (methyl ester, phosphate, mPEG, phosphoethanolamine, EA, DMEDA, PEHA), using standard activation procedures of carboxylic acids with thionyl chloride or EDC, or phosphorylation of surface hydroxyl groups with phosphorus oxychloride, followed by aqueous work up (referred as post-functionalization (Post-F)). All the CDs described herein were purified by extensive dialysis over 24 to 48 h, through a membrane with appropriate MWCO (100-500, 1,000, 3,500, or 12,000 Da).

**Table 1**: Description of the CD library

| | Carbonization procedure | Passivation reagent | Reagent ratio (w/w) | Zêta potential (mV) | Size (nm) | Hydrodynamic diameter (nm) | Aggregation in culture medium | Nitrogen (%) | Carbon (%) | Hydrogen (%) | Viability loss at 200 µg/mL (%) | EC50 (CI95%) (µg/mL) |
|---|---|---|---|---|---|---|---|---|---|---|---|---|
| **CD (-)** | | | | | | | | | | | | |
| CD1 | MW | - | - | -38.5 ± 1.9 | 28.5 | 24.7 ± 1.7 | none | 9.5 | 39.6 | 6.1 | 4.0 ± 6.8 | - |
| CD2 | MW | - | - | -19.4 ± 2.0 | 14.1 | 63.2 ± 4.9 | + | 4.1 | 23.6 | 3.6 | 14.1 ± 6.2 | - |
| CD3 | Post-F | - | - | -17.0 ± 2.6 | 36.1 | 39.1 ± 8,5 | none | 2.7 | 20.2 | 3.1 | 19.1 ± 9.9 | - |
| CD4 | Pyro | - | 1:3 | -16.8 ± 0.6 | 28.9 | 45.2 ± 3,5 | none | 0 | 45.7 | 6.3 | 6.8 ± 3.8 | - |
| CD5 | Post-F | - | - | -38.9 ± 2.4 | 14.1 | 21.7 ± 0.9 | none | 0 | 7.2 | 2.3 | 4.8 ± 4.2 | - |
| CD6 | Post-F | PEG550 | - | -20.1 ± 0.2 | 16.1 | 67.2 ± 2.6 | + | 1.1 | 48 | 7.8 | 13.7 ± 2.8 | - |
| CD7 | Post-F | PhosphoEA | - | -22.9 ± 1.5 | 15.9 | 36.5 ± 3.1 | + | 4.1 | 9.3 | 4.0 | 8.2 ± 2.3 | - |
| CD8 | Post-F | EA | - | -11.1 ± 0.8 | 14.4 | 283.7 ± 22.2 | none | 10.4 | 31.7 | 6.7 | 3.2 ± 4.3 | - |
| CD9 | MW | bPEI25k | 4:1 | -26.5 ± 1.5 | n.d. | 86,2 ± 1.0 | + | 12.9 | 44.5 | 7.0 | 11.7 ± 8.8 | - |
| **CD (+)** | | | | | | | | | | | | |
| CD10 | Pyro | EA | 1:3 | +16.7 ± 0.5 | 16.0 | 157.8 ± 29.1 | ++ | 11.1 | 43.4 | 5.7 | 21.8 ± 3.8 | - |
| CD11 | Post-F | DMEDA | - | +13.7 ± 0.9 | 23.9 | 79.2 ± 7.4 | none | 12.4 | 26.2 | 7.5 | 32.5 ± 3.3 | - |
| CD12 | Pyro | DMEDA | 1:1.4 | +21.0 ± 1.5 | 12.6 | 43.9 ± 2.4 | ++ | 12.8 | 35.6 | 7.0 | 37.2 ± 5.0 | - |
| CD13 | Pyro | DMEDA | 1:4 | +28.8 ± 2.2 | n.d. | 16.7 ± 1.4 | + | 15.3 | 47.0 | 7.0 | 9.9 ± 2.5 | - |
| CD14 | Pyro | DMEDA + PEG550 | 1:3:3 | +26.9 ± 1.6 | 16.3 | 17.7 ± 0.9 | + | 2.4 | 49.0 | 8.5 | 5.9 ± 0 .1 | - |
| CD15 | Pyro | DETA | 1:1.7 | +4.8 ± 0.5 | n.d. | 87.2 ± 4.5 | none | 19.5 | 35.5 | 7.3 | 3.1 ± 4.3 | - |
| CD16 | Pyro | DETA | 1:4 | +17.7 ± 0.8 | n.d. | 71.7 ± 11.2 | none | 19.5 | 44.5 | 6.4 | 9.7 ± 2.0 | - |
| CD17 | Post-F | PEHA | - | +21.9 ± 2.1 | 12.4 | 20.8 ± 2.0 | + | 13.9 | 27.0 | 7.3 | 35.3 ± 8.5 | - |
| CD18 | Pyro | PEHA | 1:4 | +20.6 ± 1.2 | 17.9 | 19.1 ± 2.0 | none | 12.3 | 26.9 | 7.4 | 28.3 ± 8.5 | - |
| CD19 | Pyro | PEHA + PEG550 | 1:3:3 | +25.7 ± 1.0 | 17.5 | 29.1 ± 1.1 | + | 7.2 | 43.0 | 7.9 | 25.6 ± 0.9 | - |
| CD20 | Pyro | PEHA + PEG5000 | 1:3:3 | +20.6 ± 0.6 | 13.4 | 21.2 ± 2.6 | + | 0.7 | 49.1 | 8.7 | 10.2 ± 0.2 | - |
| CD21 | MW | bPEI600 | 1:2 | +36.7 ± 2.0 | n.d. | 10.2 ± 1.1 | ++ | 14.9 | 32.4 | 6.9 | 97.6 ± 0.2 | 19.5 (18.2-21.0) |
| CD22 | MW | bPEI600 | 1:4 | +23.9 ± 2.0 | 39.5 | 10.1 ± 0.4 | ++ | 14.6 | 29.0 | 7.4 | 98.3 ± 0.1 | 34.2 (31.2-37.4) |
| CD23 | Pyro | bPEI600 | 1:2 | +30.1 ± 1.4 | 18.9 | 17.0 ± 1.7 | + | 15.1 | 36.7 | 7.0 | 97.4 ± 0.2 | 49.5 (46.1-53.1) |
| CD24 | Pyro | bPEI600 | 1:4 | +26.8 ± 2.6 | 14.2 | 16.7 ± 2.6 | + | 14.1 | 29.4 | 7.3 | 78.9 ± 0.6 | 92.2 (85.7-99.3) |
| CD25 | ST | bPEI600 | 1:2 | +22.1 ± 2.4 | 14.6 | 44.3 ± 4.9 | none | 12.5 | 25.3 | 7.6 | 16.8 ± 4.6 | - |
| CD26 | ST | bPEI600 | 1:4 | +22.3 ± 3.8 | 14.1 | 76.9 ± 1.7 | none | 14.8 | 27.0 | 7.3 | 0.2 ± 0.7 | - |
| CD27 | MW-ST | bPEI600 | 1:2 | +22.6 ± 1.9 | n.d. | 15.8 ± 3.0 | + | 13.1 | 26.2 | 7.3 | 0.3 ± 1.6 | - |
| CD28 | MW-ST | bPEI600 | 1:4 | +22.1 ± 4.1 | 16.5 | 36.1 ± 1.5 | none | 14.1 | 27.0 | 7.4 | 0.7 ± 1.4 | - |
| CD29 | Pyro | L-PEI2k | 2:1 | +37.4 ± 1.0 | n.d. | 11.2 ± 1.5 | + | n.d. | n.d. | n.d. | 51.6 ± 5.9 | - |
| CD30 | Pyro | bPEI2k | 1:4 | +31.7 ± 2.1 | n.d. | 15.4 ± 1.1 | ++ | 18.9 | 37.6 | 8.3 | 98.7 ± 0.2 | 23.2 (21.1-25.4) |
| CD31 | MW | bPEI25k | 2:1 | +5.4 ± 0.2 | n.d. | 72.6 ± 37.8 | ++ | 14.2 | 43.8 | 7.1 | 27.6 ± 6.9 | - |
| CD32 | ST | bPEI25k | 2:1 | +6.0 ± 2.2 | 5.5 | 10.4 ± 0.2 | ++ | 12.1 | 28.9 | 7.2 | 97.7 ± 0.3 | 20.9 (17.3-25.2) |
| CD33 | MW | bPEI25k | 1:2 | +33.1 ± 2.2 | 13.9 | 10.3 ± 0.8 | ++ | 15.4 | 28.3 | 7.4 | 97.2 ± 0.2 | 16.1 (13.9-18.6) |
| CD34 | MW | bPEI25k | 1:4 | +36.7 ± 1.8 | n.d. | 27.9 ± 0.7 | ++ | 13.5 | 39.0 | 6.5 | 96.6 ± 0.4 | 35.3 (31.6-39.5) |
| CD35 | Pyro | bPEI25k | 1:4 | +33.4 ± 2.2 | n.d. | 13.0 ± 0.7 | ++ | 18.2 | 42.4 | 8.1 | 98.2 ± 0.0 | 13.7 (11.9-15.6) |

(-) : not applicable ; (n.d.) : not determined ; (+) : partially aggregated ; (++) : aggregated

300

*3.2. Physicochemical characterization of CDs*

The charge, size, and elemental composition of the CDs were determined as described in the Materials and Methods section. Data are presented in Table 1 **and Figure 2**. Among the 35 NPs, 9 exhibited a negative charge with zeta potential in between -11.1 ± 0.8 and -38.9 ± 2.4 mV, whereas 26 NPs were positively charged with zeta potential ranging from +4.8 ± 0.5 to +37.4 ± 1.0 mV **(Table 1)**. CD size (TEM) and hydrodynamic diameter (DLS) ranged from 5.5 to 39.5 nm and from 10.1 ± 0.4 to 283.7 ± 22.2 nm, respectively **(Figure 2 and Table 1).** Besides, CD nitrogen, carbon and hydrogen contents were in between 0 and 19.5 %, 7.2 and 49.1%, and 2.3 and 8.7%, respectively (Table 1).

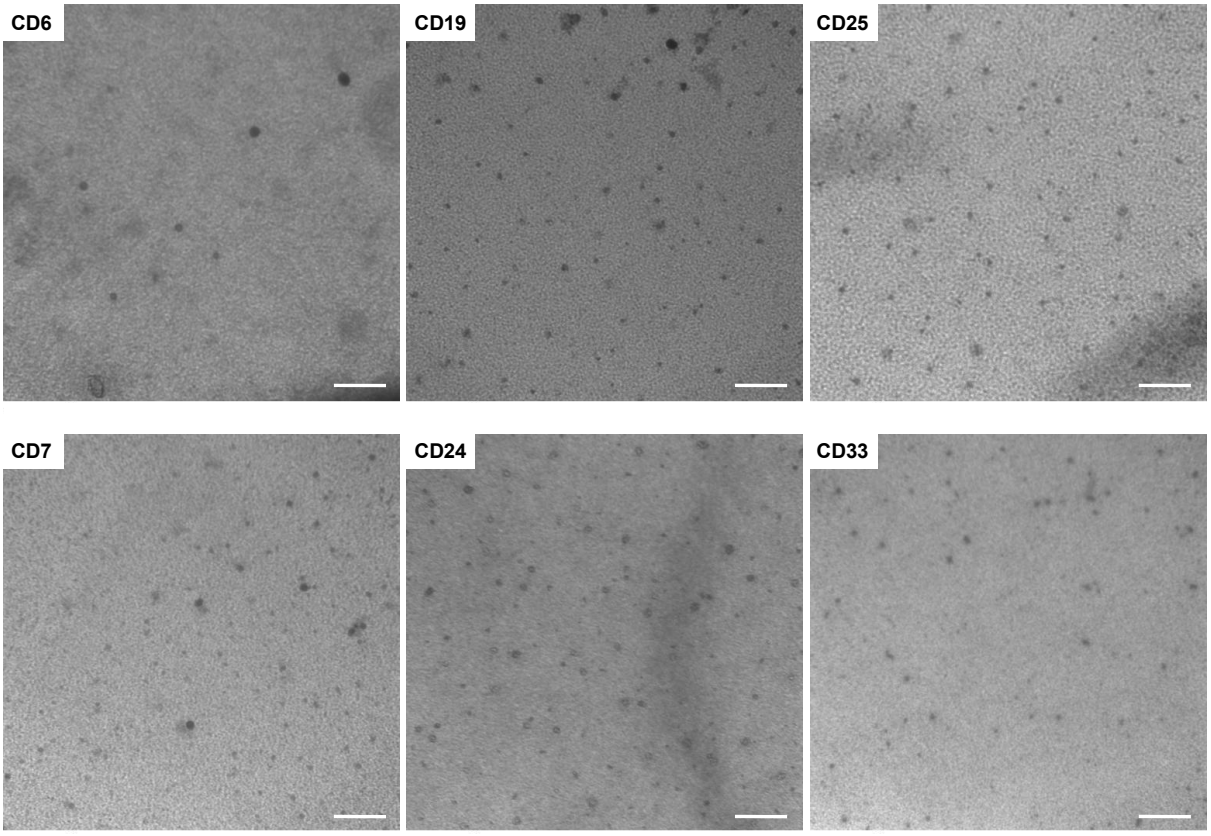


**Figure 2:** Representative TEM images of some selected CDs of the library (scale bar = 200 nm).

When entering in contact with biological fluids, nanomaterials may form aggregates or agglomerates due to ionic strength, pH or protein adsorption (Stark, 2011). To evaluate the tendency of our CDs to form such assemblies in our experimental conditions, we measured their hydrodynamic diameter in complete culture medium containing 10% foetal bovine serum. Many CDs tended to aggregate, while some remained well dispersed when in culture medium (Table

1). The aggregation was more or less pronounced, so that the CDs could be sorted in 3 groups: 1-"non aggregated" CDs, with a hydrodynamic diameter remaining less than 100 nm; 2-"partially aggregated" CDs, with a diameter in between 100 and 500 nm; and 3-"aggregated" CDs, with a diameter greater than 500 nm or out of the apparatus measurement range (Table 1). Stability and aggregation properties of nanoparticles depend on the functional groups (nature, density, and distribution/accessibility) that are displayed at the surface. Carbonization of organic materials is a temperature- and time-controlled process, the formation of extended $sp^2$-hybridized aromatic domains in the CD core and decarboxylation at the surface being favored at high temperature. Depending on the synthetic procedure and organic starting materials that were used, pyrolysis was not carried out at the same temperature and was not performed for the same duration. As a consequence, heteroatom distribution at the surface and inside the carbogenic core of the particles may significantly vary. Especially, "internal" nitrogen atoms (*i.e.*, those in the nanoparticle core) and pyridinic ones (pKa < 6) favored by high temperature and extended reaction time are less contributing to the net positive charge of the nanoparticles than graphitic ones (pKa > 9) displayed at the surface. Furthermore, it has been shown that the concentration of titratable species (*e.g.*, amines and carboxylic acids) at an interface may have a major effect on their ionization state (Pierrat and Lebeau, 2015). Considering the number of variables involved in the preparation of the CD library described herein (activation mode, temperature, reaction duration, carbon source, passivation reagent, reagent stœchiometry, solvent, pH), it was very difficult to identify specific trends and no rationale for the relationship between synthetic procedures and aggregation properties in culture medium could be proposed.

*3.3. Effect of CDs on cell viability*

To analyze the relationship between physicochemical characteristics of CDs and their safety, we assessed loss of cell viability evoked by the nanomaterials in PMA-activated THP-1 cells, as a model of human macrophages. Different cellular models can be used to explore the safety of engineered NPs. These models can be selected according to potential route of administration of the nanomaterials or organs of delivery after body absorption. In the present study, macrophages were selected as they are major players of the body defense against particles which makes them a main target for particles. Besides, several studies have shown that macrophages are more sensitive to the toxicity of nanoparticles than other cell types such as pulmonary epithelial cells (Lanone et al., 2009; Foldbjerg et al., 2013; Breznan et al., 2017). Macrophages are therefore more suitable for evidencing difference of toxicity between particles, which is the scope of our study.

The cells were exposed for 24 h to increasing concentrations of CDs (3 to 200 µg/mL) and cell viability was assessed by mitochondrial activity measurements (MTT assay). We then draw concentration-response curves for each CD, and determined cell viability loss at the highest concentration tested (200 µg/mL), as well as EC50 and EC20, when the determination was possible. These data are listed in Table 1 and displayed on Figure 3.

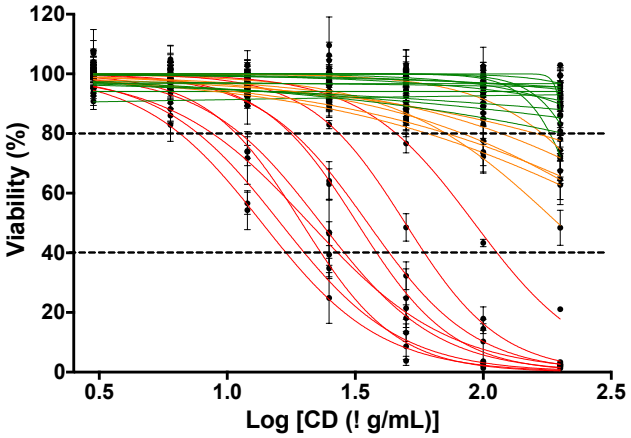


**Figure 3:** Cytotoxicity of the CD library. The cells were incubated with increasing concentrations of CDs (3-200 µg/mL). Cell viability was assessed at 24 h using the MTT assay and expressed as percentage when compared to untreated control cells. Results are means ± SEM of n=2 to 9 experiments. Green curves: CDs triggering less than 20% viability loss at 200 µg/mL. Orange curves: CDs triggering viability loss in between 20 and 60% at 200 µg/mL. Red curves: CDs triggering viability loss greater than 60% at 200 µg/mL.

The 35 CDs exhibited various levels of cytotoxicity (Figure 3 and Table 1). They were sorted in 3 groups: 1-toxic NPs (9 CDs inducing viability loss at 200 µg/mL greater than 60% with EC50=13.7 to 92.2 µg/mL (see individual EC50 and 95% confidence interval (CI95%) values in Table 1, concentration-reponse curves in red on Figure 3), 2-weakly toxic NPs (7 CDs triggering viability loss at 200 µg/mL in between 20 and 60% with EC20=5.8 to 177.3 µg/mL (EC20 not shown, concentration-response curves in orange on Figure 3) and 3-harmless NPs (19 CDs inducing viability loss less than 20% at 200 µg/mL, concentration-response curves in green on Figure 3). Very few comparative toxicity studies are available so far in the literature for CDs. Havrdova *et al.* compared the cytotoxicity of 3 kinds of CDs produced from candle soot, namely pristine CDs, CDs passivated with PEG, and CDs passivated with PEI (Havrdova et al., 2016). The authors found significant differences in toxicity among the 3 NPs using fibroblasts and several toxicity endpoints, the PEI-passivated CDs being the more toxic. Wang *et al.* assessed changes in vability of MCF-7 and HT-29 cells in response to 4 CDs prepared from various precursors and passivated with different molecules

(Wang et al., 2011). Cytotoxicity of the CDs appeared to depend on the nature of the surface passivation molecules. On their hand, Cailotto *et al.* compared the cytotoxicity towards Hela cells of 3 CDs prepared from different precursors, namely fructose, glucose and ascorbic acid (Cailotto et al., 2018). CDs made from fructose were toxic, while those made from glucose and ascorbic acid showed good biocompatibility. The fact that the toxicity of the CDs investigated herein was assessed in a single viability assay, using the MTT assay which has been reported to give some interference with carbon materials (Wörle-Knirsch et al., 2006), could be questioned. However, interference of carbon nanomaterials with the MTT assay was observed with hydrophobic SWCNT, and it is not surprising that SWCNT (even when treated with 1 % SDS solution prior to cell contact) adsorb hydrophobic MTT-formazan crystals formed in the MTT reaction and thus interfere with the normal readout of the assay. In the case of hydrophilic nanoparticles like CDs, such an interference is not expected. In agreement with this hypothesis, we have previously reported that CDs exhibited similar cytotoxicity profile with similar EC50, in THP-1 cells when using the neutral red and the MTT assays (Ronzani et al., 2019). Beside, most of the toxicity work on CDs cited above used MTT as viability assay. All together, our study is the first one to explore the safety of a large library of CDs. In agreement with the above mentionned studies, our data confirm the hypothesis that the biocompatibility of CDs cannot be generalized, and that factors influencing the toxicological properties of the NPs deserve investigation.

### *3.4. Relationship between hydrodynamic diameter or aggregation state in culture medium and toxicity*

Decreasing the size of materials leads to an exponential increase in their surface area, favoring interactions with their environment and biological activity (Nel et al., 2006). By the way, the smaller particles are considered as more toxic towards cells than larger ones, which has been established for various kinds of NPs (Midander et al., 2009; Napierska et al., 2009; Park et al., 2011). However, some conflicting data can be found in the literature suggesting that the relationship between particle size and toxicity is not straightforward (Gatoo et al., 2014; Luyts et al., 2013). To analyze the relationship between size and safety of CDs, we plotted viability loss evoked by the NPs at 200 µg/mL against their hydrodynamic diameter in 1.5 mM NaCl pH 7.4. Although moderate, a significant negative correlation (Pearson's r = -0.53; $p$<0.01) was found between these two parameters (Figure 4A). All toxic CDs except **CD34** thus had a hydrodynamic diameter in the range of 10-20 nm, whereas the size of harmless and weakly toxic CDs spanned over a wider range, *i.e.* 10-100 nm, suggesting that smaller particles are more toxic that larger

ones. These data are in agreement with the hypothesis that when the size of NPs decreases, their capacity to interact with their environment, and therefore their toxicity, increases.

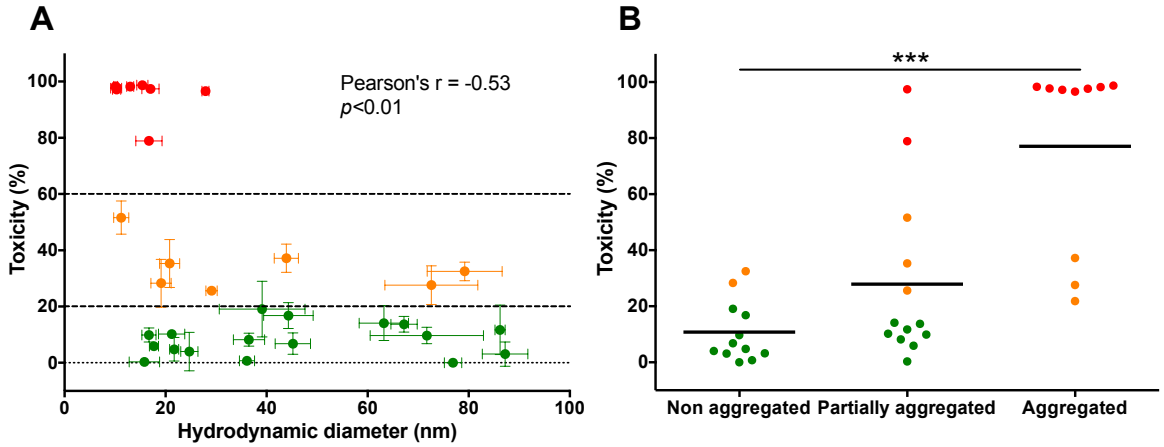


**Figure 4:** Relationship between toxicity and CD hydrodynamic diameter (A) or aggregation state in culture medium (B). Scatter representations were obtained by plotting percentage of viability loss induced by 200 µg/mL CDs and CD hydrodynamic diameter in 1.5 mM NaCl pH 7.4 (A) or CD aggregation state in complete culture medium (B). Green dots: harmless CDs ; Orange dots: weakly toxic CDs ; Red dots: toxic CDs. (A) Data are represented as mean ± SEM (toxicity) or SD (hydrodynamic diameter). The Pearson's test was applied to evaluate the correlation and determine the Pearson's r. (B) Statistical differences between groups were determined by one way ANOVA followed by the Dunnett's test. ***$p$<0.001 when compared to the non aggregated group.

Some CDs tend to aggregate in culture medium (see section 3.2. and Table 1), which could affect their biological activity. So, we plotted cytotoxicity of the NPs against their aggregation state, namely non aggregated, partially aggregated and aggregated (Figure 4B). Non toxic CDs were dispersed or partially aggregated in culture medium (green dots on Figure 4B). Weakly toxic CDs were found in the 3 groups (orange dots on Figure 4B). In contrast, all toxics CDs were in the aggregated group, except **CD23**, **CD24** and **CD29** that were partially aggregated (red dots on Figure 4B). Although aggregation may drastically influence the biokinetic of NPs *in vivo* (Stark, 2011) and could be responsible among others of a NP-induced inflammatory response in lung (Shin et al., 2015), its impact at the cellular level remains unclear. Indeed, whereas aggregation of NPs may mechanically favor their interaction with cells (through a sedimentation process), it may affect the mechanisms by which they enter cells and by the way their toxicity. Besides, aggregates when too large to be taken up by cells may reduce NP bioavailability and

initiate frustrated phagocytosis in specific cells such as macrophages (Albanese and Chan, 2011; Luyts et al., 2013). In the present study, aggregation of CDs was clearly associated with toxicity.

### *3.5. Relationship between charge and toxicity*

Surface charge is well known to influence nanomaterial biocompatibility, a positive zeta potential being generally associated with higher toxicological risks (Gatoo et al., 2014; Luyts et al., 2013). To analyze the relationship between charge and safety of the NPs, we plotted viability loss evoked by the CDs at 200 µg/mL against zeta potential values. As shown on Figure 5A, negatively charged CDs were all harmless, whereas cationic ones were either harmless, weakly toxic, or toxic. A significant positive correlation was found between CD toxicity and zeta potential values. Although this correlation is moderate (Pearson's r = 0.53; $p<0.001$), all the toxic CDs except one **(CD32)** had a charge greater than +20 mV.

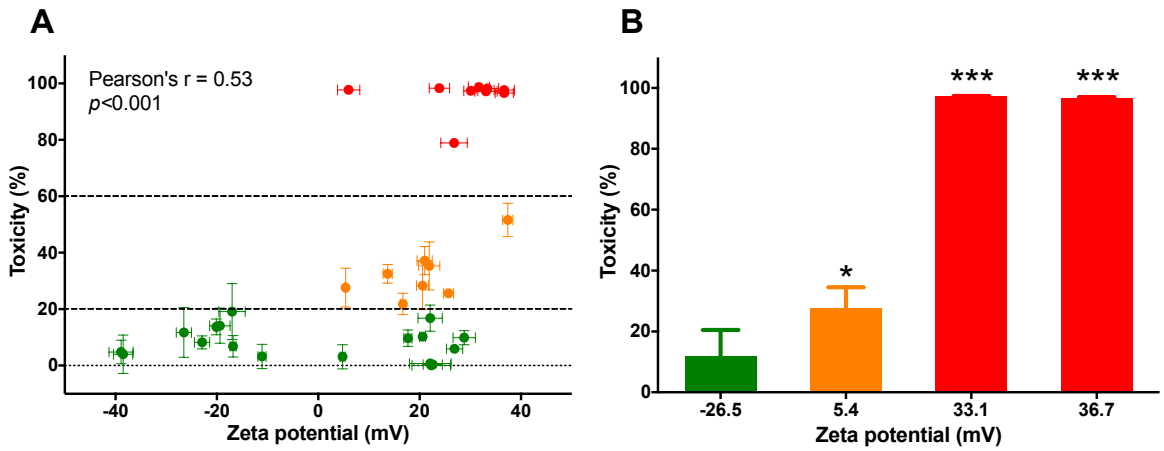


**Figure 5:** Relationship between the charge and toxicity of CDs. (A) Scatter representation obtained by plotting cytotoxicity data against zeta potential values for all CDs. Green dots: harmless CDs ; Orange dots: weakly toxic CDs ; Red dots: toxic CDs. (B) Bar charts obtained by plotting cytotoxicity data against zeta potential values for **CD9** (green bar), **CD31** (orange bar), and **CD33** and **CD34** (red bar). In the two representations, toxicity is expressed as the percentage of viability loss at 200 µg/mL CDs. Data are mean ± SEM (toxicity) or SD (zeta potential). (A) The Pearson's test was applied to evaluate the correlation and determine the Pearson's r. (B) Statistical differences between groups were determined by one way ANOVA followed by the Dunnett's test. *$p<0.05$ and ***$p<0.001$ when compared to untreated control cells.

To strengthen our analysis of the relationship between charge and safety of CDs, we compared the toxicity of **CD9**, **CD31**, **CD33** and **CD34** (Figure 5B). These CDs were produced from the same reagents (citric acid and bPEI25k, in various w/w ratios: 4:1, 2:1, 1:2 and 1:4, respectively) through the same synthesis process. They exhibited similar carbon, hydrogen and nitrogen contents, but differed in their zeta potential (Table 1). The comparison clearly showed that a cationic charge is an important factor in determining CD toxicity (Figure 5B), although a contribution of size can not be totally ruled out, since hydrodynamic diameters of **CD33** and **CD34** are smaller than **CD9** and **CD31** ones (10.3 and 27.9 nm *vs*. 86.2 and 72.6 nm, respectively). In the literature, a similar role of the cationic charge has been reported for various kinds of NPs, including silicon- (Shahbazi et al., 2013), silver- (El Badawy et al., 2011), or polystyrene-based NPs (Kim et al., 2016), and CNTs (Li et al., 2013). Greater toxicity of cationic NPs is attributed to their greater capacity to interact with the cell membrane and/or to bind proteins at their surface due to attractive electrostatic interactions with negatively charged phospholipids or proteins (Mahmoudi et al., 2011; Sharifi et al., 2012). In agreement with our data, CDs displaying a net positive charge were reported to be more toxic towards cultured fibroblasts than negatively charged CDs (Havrdova et al., 2016). This observation was made however by comparing one kind of negative CDs to one kind of positive one. In our study conducted on 26 cationic NPs, we found that several positive CDs exhibited no or weak toxicity, while having a marked positive zeta potential (for example **CD13**, **CD14**, **CD19**, **CD25**-**CD29**). Some of these CDs likely display PEG decoration which could explain their lower toxicity (**CD13** and **CD19**), but not all of them, suggesting the existence of other important factors in governing CD toxicity. So, thanks to investigations on an extended NP library, we were able to show that a positive charge is not sufficient to predict CD toxicity. Surface charge is considered to have a great importance for cell uptake of NPs and consequently NP toxicity. Thus, on a mechanistic point of view, it would have been interesting to assess CD internalization in the present study. However, although CDs exhibit intrinsic fluorescence properties, their quantum yield varies according to their chemical composition, which makes difficult the direct comparison of their internalization rate.

### *3.6. Relationship between chemical composition and toxicity*

The chemical composition of NPs also influences their toxicity (Gatoo et al., 2014). To analyze the relationship between composition and safety of CDs, we plotted viability loss evoked by the NPs at 200 µg/mL against their carbon, hydrogen and nitrogen content (Figure 6). We did not

found any correlation between carbon content (Figure 6A, Pearson's r = 0.01 ; $p$>0.05) or hydrogen content (data not shown, Pearson's r = 0.25 ; $p$>0.05) and the toxicity of CDs. However, a significant positive relation was found with the nitrogen content, even if this relation is weak (figure 6B ; Pearson's r = 0.44 ; $p$<0.01). This is fully consistent with our previous observation of a positive correlation between CD toxicity and zeta potential, as positive charges at the surface of CDs result from the protonation at physiological pH of amine groups displayed at the surface of the particles. Though all nitrogen atoms in the CD structure may not be fully available for titration (*i.e.* those in the CD core structure where diffusion of protons may be sterically prevented or those with a lower p$K_a$ value, e.g., pyridinic or pyrrolic nitrogen atoms), it can be reasonably expected that the higher the nitrogen content, the higher the positive charge of the particles.

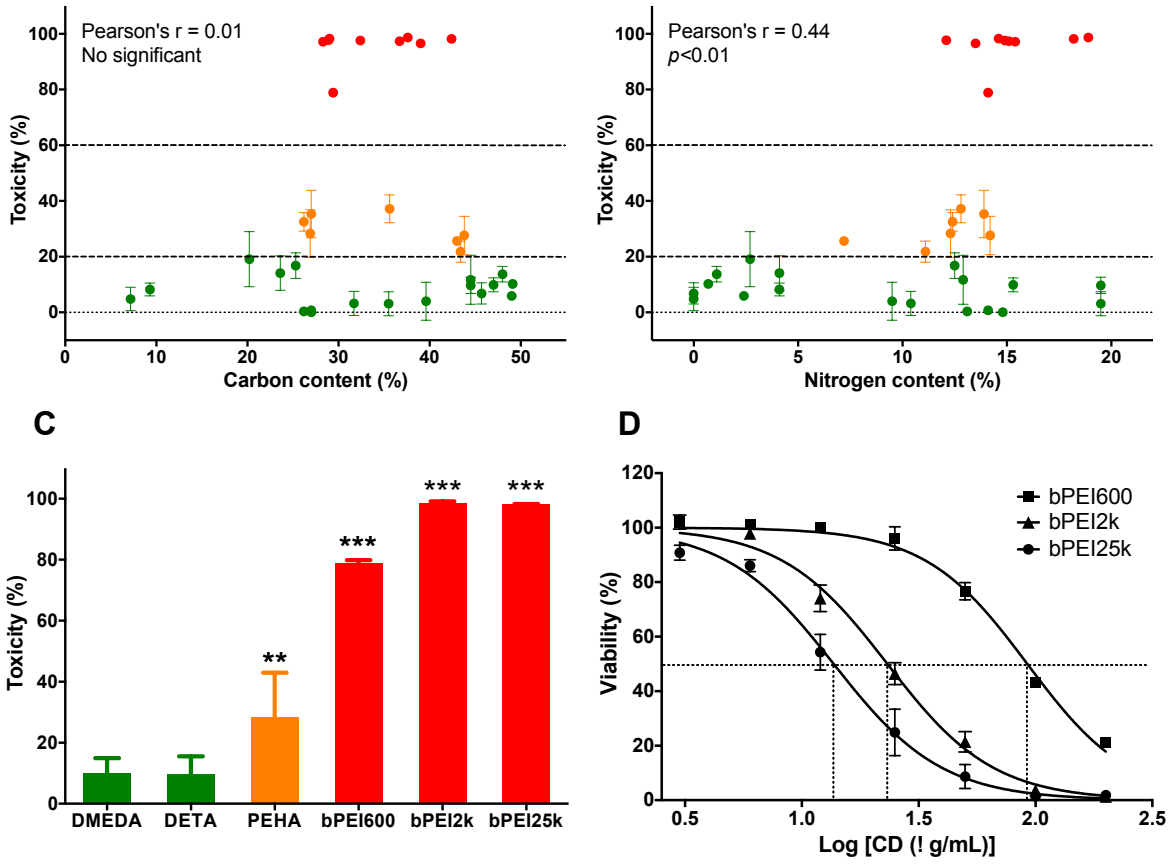


**Figure 6:** Relationship between CD composition and toxicity. Scatter representations obtained by plotting percentage of viability loss induced by CDs (200 µg/mL) against carbon (A) or nitrogen (B) CD content. (C) Percentage of cell viability loss induced by CDs prepared from pyrolysis of citric acid and DMEDA (**CD13**), DETA (**CD16**), PEHA (**CD18**), bPEI600 (**CD24**), bPEI2k (**CD30**) or bPEI25k (**CD35**), when incubated with cells at 200 µg/mL. (D) Concentration-

reponse curves of bPEI600- (**CD24**), bPEI2k- (**CD30**) and bPEI25k- (**CD35**) based CDs (3-200 µg/mL), pointing out EC50. Data are means ± SEM of n=2-9 experiments. (A and B) Green dots: harmless CDs ; Orange dots: weakly toxic CDs ; Red dots: toxic CDs. The Pearson's test was applied to evaluate the correlation and determine the Pearson's r. (C) Green bars: harmless CDs ; Orange bars: weakly toxic CDs ; Red bars: toxic CDs. Statistical differences between groups were determined by one way ANOVA followed by the Dunnett's test. $^{**}p<0.01$ and $^{***}p<0.001$ when compared to untreated control cells.

Nitrogen-containing passivation agents with increasing number of protonatable (titratable) amino groups (DMEDA, DETA, PEHA and PEI of various length) were used to produce cationic CDs, which could explain the correlation between toxicity and nitrogen content. So to strengthen our correlation study, we focused our analysis on CDs prepared from citric acid and nitrogen-containing passivation agent using the same synthesis mode (pyrolysis) and reagent weight to weight ratio (1:4), namely **CD13**, **CD16**, **CD18**, **CD24**, **CD30** and **CD35**. These CDs had a positive zeta potential in between +17.7 and +33.4 mV and a similar hydrodynamic diameter ranging from 13.0 to 19.1 nm, except **CD16** which diameter was 71.7 nm. As shown on Figure 6C, although being cationic, DMEDA- (**CD13**) and DETA- (**CD16**) based CDs exhibited no toxicity, which is in agreement with our above hypothesis that a cationic charge is not sufficient to predict CD toxicity. By contrast, the longer the chain of the passivation agent, and by the way the number of protonatable amino groups, the higher the toxicity (Figure 6C). This was even more clearly observed with PEI-based CDs since ranking of these CDs according to EC50 values was as follows: bPEI25k (**CD35**, EC50=13.7 µg/mL) < bPEI2k (**CD30**, EC50=23.2 µg/mL) < bPEI600 (**CD24**, EC50=92.2 µg/mL) (Figure 5D). After their cell entry, cationic CDs can traffick to the lysosomes (Ronzani et al., 2018; Wu et al., 2017). At the acidic lysosomal pH, difference in number of protonated amino groups should result in difference in the density of positive charges at or close to the CD surface. Depending on the geometry of the particles, such differences may not necessarily translate into large variations of zeta potential that is invariably used to characterize the NP charge. Indeed, immediately surrounding the NP is a layer of tightly associated ions (Stern layer), opposite in charge to the surface of the particle. Surrounding the Stern layer is a second layer of loosely associated ions. The point at which this second layer of ions moves with the NP as a single entity is termed the slipping plane, and zeta potential is defined as the potential at this slipping plane, separating the NP and associated ions from the ions of the bulk dispersing medium under an applied electric field. Consequently, particles with similar zeta potential may display quite different charge distribution, which can have a possible impact on biomolecule adsorption at the NP surface (adsorption rate, composition, and

exchange rate) and can translate into differences in toxicity, especially towards lysosomes. This mechanistic hypothesis needs further investigations. Anyway, our data suggest that the global density of positive charges of CDs, rather than the value of their zeta potential at their surface is predictive of the CD toxicity.

*3.7. Impact of pegylation on CD toxicity*

Passivation with PEG chains has been described to significantly increase NP blood circulating time and reduce their toxicity *in vivo* and *in vitro* by preventing NP opsonization and recognition by the immune system (Suk et al., 2016). CDs developed for imaging purpose are often PEG-passivated NPs and thus characterized by suitable biocompatibility (Wang et al., 2011; Yang et al., 2009). In the present study, we wondered whether pegylation could mitigate toxicity of CDs. To assess this issue, we compared the toxicity of **CD18** (bare CDs) to that of **CD19** (CDs with PEG550 decoration) and **CD20** (CDs with PEG5000 decoration). These NPs of similar cationic charge (+20.6, +25.7 and +20.6 mV, respectively) and hydrodynamic diameter (19.1, 29.1 and 21.2 nm, respectively) were produced by dry pyrolysis of citric acid and PEHA in absence or in the presence of PEG550 or PEG5000. As shown on Figure 7, provided the PEG chain was long enough, pegylation did help in reducing CD toxicity. These data are in agreement with those reported by other groups for NPs obtained by pegylation of CDs from candle soot (Havrdova et al., 2016).

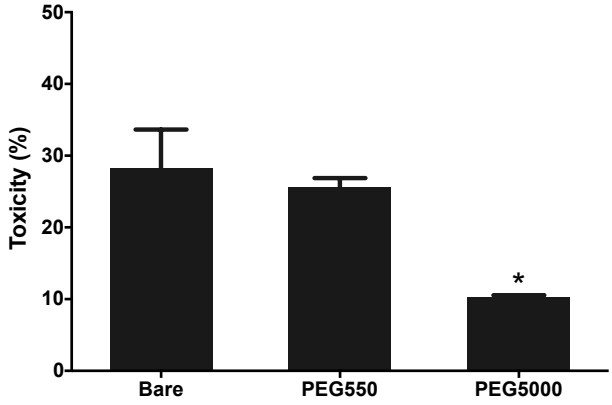

**Figure 7:** Impact of pegylation on CD toxicity. Cytotoxicity of **CD18** (bare CDs), **CD19** (CDs with PEG550 decoration) and **CD20** (CDs with PEG5000 decoration) was expressed as percentage of viability loss at 200 µg/mL CDs. Data are means ± SEM of n=4 to 6 experiments. Statistical differences between groups were determined by one way ANOVA followed by the Dunnett's test. *$p$<0.05 whan compared to bare CDs.

*3.8. Impact of the mode of synthesis on CD toxicity*

In order to generate NP diversity, we synthesized our CD library using various carbon sources, passivating agents, and reagent ratios. We used as well various carbonization conditions as it was recently reported they lead to significant variation in properties of the resulting materials (Claudel et al., 2019; Krysmann et al., 2012; Xiong et al., 2017), and by the way may influence the NP safety. To analyze the relationship between the mode of synthesis of CDs and their safety, we focused our analysis on **CD21** to **CD28**. These CDs were produced from different ratios of citric acid and bPEI600 (1:2 or 1:4) using different carbonization procedures (MW, Pyro, ST or MW-ST). They all had a cationic charge in the range of +22.1 to +36.7 mV, and a hydrodynamic diameter around 10-15 nm, except **CD25** (44.3 nm), **CD26** (76.9 nm) and **CD28** (36.1 nm). Among these 8 CDs, those produced by the microwave-assisted solvothermal (MW-ST) and conventional solvothermal (ST) methods exhibited no or low toxicity whatever the reagent ratio (Figure 8A). In contrast, the 4 CDs (**CD21 to CD24**) produced by solvent-free pyrolysis (Pyro) or under microwave irradiation at atmospheric pressure (MW) were toxic, again whatever the reagent ratio (Figure 8A). The carbonization process may have an impact on CD internal nanostructure, potentially conditioning their biological effect. Yet, the nanomaterial structure, such as the crystal structure, was shown to influence NP toxicity as reported for $TiO_2$ or ZnS NPs (Gatoo et al., 2014). Comparison of the concentration-toxicity curves for these 4 toxic CDs showed that whatever the mode of synthesis, the CDs prepared from the 1:2 ratio were more toxic than those prepared from the 1:4 ratio (Figure 8B). Furthermore, microwave irradiation of the reagents at atmospheric pressure (MW) yielded CDs that revealed more harmful than those obtained through pyrolysis of the precursors under solvent-free conditions (Pyro). Therefore, at least for citric acid- and bPEI600-based NPs, synthesis mode and ratio of the reagents appeared to significantly influence toxicity of the CDs thereof. This last point underlines not only the complexity of predicting CD safety, but also the difficulty in comparing data from different groups, as a very large panel of procedures is currently used to synthesize CDs.

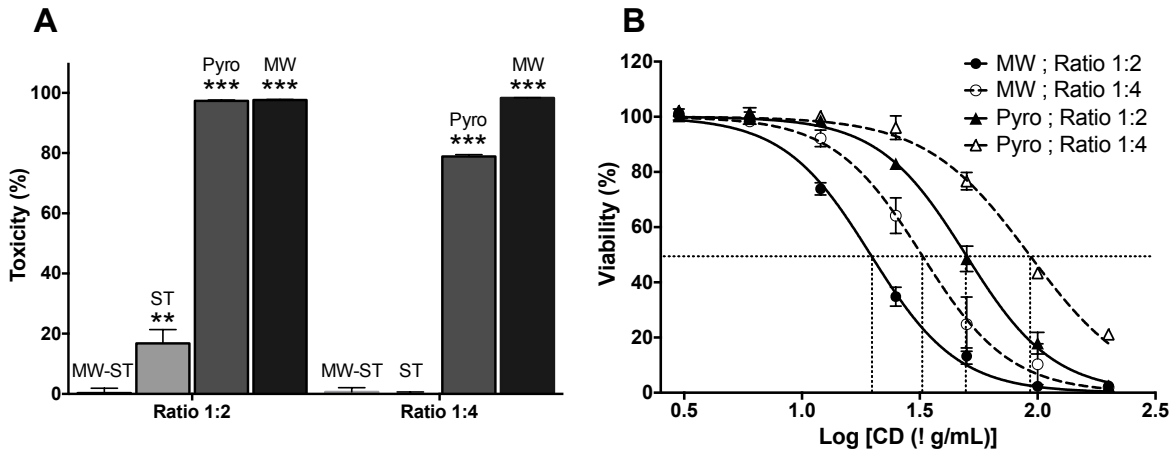


**Figure 8:** Impact of the mode of synthesis on CD toxicity. (A) Cytotoxicity expressed as percentage of viability loss at 200 µg/mL of citric acid- and PEI600-based CDs prepared from different reagent ratio by four different carbonization procedures. (B) Concentration-response curves of the 4 toxic CDs (**CD21 to CD24**, 3-200 µg/mL) pointing out EC50. Statistical differences between groups were determined by two-way ANOVA followed by the Dunnett's test. **$p$<0.01 and ***$p$<0.001 when compared to untreated control cells.

## 4. Conclusion

Carbon dots are emerging nanomaterials in medicine and pharmacy that are largely considered as biocompatible, although no in depth structure-safety relationship study was conducted so far. To tentatively fill in this gap, we synthesized a library of CDs, and explored toxicity profile of the NPs on macrophages. Our data showed that CDs can trigger various levels of viability loss ranging from no toxicity to high toxicity in our test conditions. This suggests that biocompatibility of CDs cannot be generalized and highlights the need for a systematic assessment of the NP safety. By analyzing structure-toxicity relationships, we found, as previously reported in the literature for other nanomaterials, that the size, charge and aggregation in culture medium influence CD toxicity. But, our study also highlighted the importance of other more specific CD parameters, such as nitrogen content, nature of the passivation agent and carbonization procedure, in CD toxicity. Altogether, not a single CD factor appears as a most important characteristic, pointing out the complexity of predicting the safety of CDs, most probably because of interplays between their different physicochemical properties.

**Acknowledgement**

The authors thank Maud Weiss and Mickaël Rapp for technical assistance in the preparation and characterization of carbon dots.

**Funding**

This work was supported by the Agence Nationale de Sécurité Sanitaire de l'alimentation, de l'environnement et du travail (ANSES - Grant number: EST-2015/1/005).

**Conflict of interest**

The authors declare that they have no conflict of interest.

**References**


Albanese, A., Chan, W.C.W., 2011. Effect of gold nanoparticle aggregation on cell uptake and toxicity. Acs Nano 5, 5478-5489.

Blas-Garcia, A., Baldovi, H.G., Polo, M., Victor, V.M., Garcia, H., Herance, J.R., 2016. Toxicological properties of two fluorescent carbon quantum dots with onion ring morphology and their usefulness as bioimaging agents. RSC Adv. 6, 30611-30622.

Breznan, D., Das, D.D., O'Brien, J.S., MacKinnon-Roy, C., Nimesh, S., Vuong, N.Q., Bernatchez, S., DeSilva, N., Hill, M., Kumarathasan, P., Vincent, R., 2017. Differential cytotoxic and inflammatory potency of amorphous silicon dioxide nanoparticles of similar size in multiple cell lines. Nanotoxicology 11, 223-235.

Cailotto, S., Amadio, E., Facchin, M., Selva, M., Pontoglio, E., Rizzolio, F., Riello, P., Toffoli, G., Benedetti, A., Perosa, A., 2018. Carbon dots from sugars and ascorbic acid: Role of the precursors on morphology, properties, toxicity, and drug uptake. ACS Med. Chem. Lett. 9, 832-837.

Claudel, M., Fan, J., Rapp, M., Pons, F., Lebeau, L., 2019. Influence of carbonization conditions on luminescence and gene delivery properties of nitrogen-doped carbon dots. RSC Adv. 9, 3493-3502.

Dou, Q., Fang, X., Jiang, S., Chee, P.L., Lee, T.-C., Loh, X.J., 2015. Multi-functional fluorescent carbon dots with antibacterial and gene delivery properties. RSC Adv. 5, 46817-46822.

Edison, T.N.J.I., Atchudan, R., Sethuraman, M.G., Shim, J.J., Lee, Y.R., 2016. Microwave assisted green synthesis of fluorescent N-doped carbon dots: Cytotoxicity and bio-imaging applications. J. Photochem. Photobiol. B 161, 154-161.

El Badawy, A.M., Silva, R.G., Morris, B., Scheckel, K.G., Suidan, M.T., Tolaymat, T.M., 2011. Surface charge-dependent toxicity of silver nanoparticles. Environ. Sci. Technol. 45, 283-287.

Emam, A.N., Loutfy, S.A., Mostafa, A.A., Awad, H., Mohamed, M.B., 2017. Cytotoxicity, biocompatibility and cellular response of carbon dots-plasmonic based nano-hybrids for bioimaging. RSC Adv. 7, 23502-23514.

Foldbjerg, R., Wang, J., Beer, C., Thorsen, K., Sutherland, D.S., Autrup, H., 2013. Biological effects induced by BSA-stabilized silica nanoparticles in mammalian cell lines. Chem. Biol. Interact. 25, 28-38.

Gatoo, M.A., Naseem, S., Arfat, M.Y., Dar, A.M., Qasim, K., Zubair, S., 2014. Physicochemical properties of nanomaterials: Implication in associated toxic manifestations. Biomed. Res. Int. 498420.

Gomez, I.J., Arnaiz, B., Cacioppo, M., Arcudi, F., Prato, M., 2018. Nitrogen-doped carbon nanodots for bioimaging and delivery of paclitaxel. J. Mat. Chem. B 6, 5540-5548.

Gong, P.W., Sun, L., Wang, F., Liu, X.C., Yan, Z.Q., Wang, M.Z., Zhang, L., Tian, Z.Z., Liu, Z., You, J.M., 2019. Highly fluorescent N-doped carbon dots with two-photon emission for ultrasensitive detection of tumor marker and visual monitor anticancer drug loading and delivery. Chem. Eng. J. 356, 994-1002.

Hassan, M., Gomes, V.G., Dehghani, A., Ardekani, S.M., 2018. Engineering carbon quantum dots for photomediated theranostics. Nano Res. 11, 1-41.

Havrdova, M., Hola, K., Skopalik, J., Tomankova, K., Martin, P.A., Cepe, K., Polakova, K., Tucek, J., Bourlinos, A.B., Zboril, R., 2016. Toxicity of carbon dots - Effect of surface functionalization on the cell viability, reactive oxygen species generation and cell cycle. Carbon 99, 238-248.

Himaja, A.L., Karthik, P.S., Singh, S.P., 2015. Carbon dots: The newest member of the carbon nanomaterials family. Chem. Rec. 15, 595-615.

Hola, K., Zhang, Y., Wang, Y., Giannelis, E.P., Zboril, R., Rogach, A.L., 2014. Carbon dots-Emerging light emitters for bioimaging, cancer therapy and optoelectronics. Nano Today 9, 590-603.

Hu, L.M., Sun, Y., Li, S.L., Wang, X.L., Hu, K.L., Wang, L.R., Liang, X.J., Wu, Y., 2014. Multifunctional carbon dots with high quantum yield for imaging and gene delivery. Carbon 67, 508-513.

Huang, D.P., Zhou, H.F., Wu, Y.Q., Wang, T., Sun, L.L., Gao, P., Sun, Y.Z., Huang, H.N., Zhou, G.J., Hu, J.F., 2019. Bottom-up synthesis and structural design strategy for graphene quantum dots with tunable emission to the near infrared region. Carbon 142, 673-684.

Kim, J., Chankeshwara, S.V., Thielbeer, F., Jeong, J., Donaldson, K., Bradley, M., Cho, W.S., 2016. Surface charge determines the lung inflammogenicity: A study with polystyrene nanoparticles. Nanotoxicology 10, 94-101.

Kim, S., Choi, Y., Park, G., Won, C., Park, Y.J., Lee, Y., Kim, B.S., Min, D.H., 2017. Highly efficient gene silencing and bioimaging based on fluorescent carbon dots in vitro and in vivo. Nano Res. 10, 503-519.

Krysmann, M.J., Kelarakis, A., Dallas, P., Giannelis, E.P., 2012. Formation mechanism of carbogenic nanoparticles with dual photoluminescence emission. J. Am. Chem. Soc. 134, 747-750.

Kwon, W., Lee, G., Do, S., Joo, T., Rhee, S.W., 2014. Size-controlled soft-template synthesis of carbon nanodots toward versatile photoactive materials. Small 10, 506-513.

Lanone, S., Rogerieux F., Geys J., Dupont A., Maillot-Marechal E., Boczkowski J., Lacroix G., Hoet P., 2009. Comparative toxicity of 24 manufactured nanoparticles in human alveolar epithelial and macrophage cell lines. Part. Fibre Toxicol. 30, 6-14.

Lategan, K., Alghadi, H., Bayati, M., de Cortalezzi, M.F., Pool, E., 2018. Effects of graphene oxide nanoparticles on the immune system biomarkers produced by RAW 264.7 and human whole blood cell cultures. Nanomaterials 8, 125.

Li, H.T., Kang, Z.H., Liu, Y., Lee, S.T., 2012. Carbon nanodots: Synthesis, properties and applications. J. Mater. Chem. 22, 24230-24253.

Li, R.B., Wang, X., Ji, Z.X., Sun, B.B., Zhang, H.Y., Chang, C.H., Lin, S.J., Meng, H., Liao, Y.P., Wang, M.Y., Li, Z.X., Hwang, A.A., Song, T.B., Xu, R., Yang, Y., Zink, J.I., Nel, A.E., Xia, T., 2013. Surface charge and cellular processing of covalently functionalized multiwall carbon nanotubes determine pulmonary toxicity. Acs Nano 7, 2352-2368.

Li, S., Guo, Z., Zhang, Y., Xue, W., Liu, Z.H., 2015. Blood compatibility evaluations of fluorescent carbon dots. Acs Appl. Mater. Interfaces 7, 19153-19162.

Liu, C.J., Zhang, P., Zhai, X.Y., Tian, F., Li, W.C., Yang, J.H., Liu, Y., Wang, H.B., Wang, W., Liu, W.G., 2012. Nano-carrier for gene delivery and bioimaging based on carbon dots with PEI-passivation enhanced fluorescence. Biomaterials 33, 3604-3613.

Luyts, K., Napierska, D., Nemery, B., Hoet, P.H.M., 2013. How physico-chemical characteristics of nanoparticles cause their toxicity: complex and unresolved interrelations. Environ Sci.-Proc. Imp. 15, 23-38.

Mahmoudi, M., Lynch, I., Ejtehadi, M.R., Monopoli, M.P., Bombelli, F.B., Laurent, S., 2011. Protein-nanoparticle interactions: Opportunities and challenges. Chem. Rev. 111, 5610-5637.

Midander, K., Cronholm, P., Karlsson, H.L., Elihn, K., Möller, L., Leygraf, C., Wallinder, I.O., 2009. Surface characteristics, copper release, and toxicity of nano- and micrometer-sized copper and copper(II) oxide particles: a cross-disciplinary study. Small 5, 389-399.

Napierska, D., Thomassen, L.C., Rabolli, V., Lison, D., Gonzalez, L., Kirsch-Volders, M., Martens, J.A., Hoet, P.H., 2009. Size-dependent cytotoxicity of monodisperse silica nanoparticles in human endothelial cells. Small 5, 846-853.

Nel, A., Xia, T., Madler, L., Li, N., 2006. Toxic potential of materials at the nanolevel. Science 311, 622-627.

Park, J., Lim, D.H., Lim, H.J., Kwon,T., Choi, J.S., Jeong, S., Choi, I.H., Cheon., J., 2011. Size dependent macrophage responses and toxicological effects of Ag nanoparticles. Chem. Commun. 47, 4382-4384.

Pierrat, P., Wang, R., Kereselidze, D., Lux, M., Didier, P., Kichler, A., Pons, F., Lebeau, L., 2015. Efficient in vitro and in vivo pulmonary delivery of nucleic acid by carbon dot-based nanocarriers. Biomaterials 51, 290-302.

Pierrat, P., Lebeau, L., 2015. Characterization of titratable amphiphiles in lipid membranes by fluorescence spectroscopy. Langmuir 31, 12362-12371.

Qian, J., Chen, J.T., Ruan, S.B., Shen, S., He, Q., Jiang, X.G., Zhu, J.H., Gao, H.L., 2014. Preparation and biological evaluation of photoluminescent carbonaceous nanospheres. J. Colloid Interface Sci. 429, 77-82.

Ray, S.C., Saha, A., Jana, N.R., Sarkar, R., 2009. Fluorescent carbon nanoparticles: Synthesis, characterization, and bioimaging application. J. Phys. Chem. C 113, 18546-18551.

Ronzani, C., Spiegelhalter, C., Vonesch, J.L., Lebeau, L., Pons, F., 2012. Lung deposition and toxicological responses evoked by multi-walled carbon nanotubes dispersed in a synthetic lung surfactant in the mouse. Arch. Toxicol. 86, 137-149.

Ronzani, C., Van Belle, C., Didier, P., Spiegelhalter, C., Pierrat, P., Lebeau, L., Pons, F., 2018. Lysosome mediates toxicological effects of polyethyleneimine-based cationic carbon dots. J. Nanopart. Res. 21,4.

Sachdev, A., Matai, I., Gopinath, P., 2014. Implications of surface passivation on physicochemical and bioimaging properties of carbon dots. RSC Adv. 4, 20915-20921.

Salieri, B., Pasteris, A., Netkueakul, W., Hischier, R., 2017. Key physicochemical properties of nanomaterials in view of their toxicity: An exploratory systematic investigation for the example of carbon-based nanomaterial. J. Nanopart. Res. 19, 116.

Shahbazi, M.A., Hamidi, M., Makila, E.M., Zhang, H.B., Almeida, P.V., Kaasalainen, M., Salonen, J.J., Hirvonen, J.T., Santos, H.A., 2013. The mechanisms of surface chemistry effects of mesoporous silicon nanoparticles on immunotoxicity and biocompatibility. Biomaterials 34, 7776-7789.

Sharifi, S., Behzadi, S., Laurent, S., Forrest, M.L., Stroeve, P., Mahmoudi, M., 2012. Toxicity of nanomaterials. Chem. Soc. Rev. 41, 2323-2343.

Shin, S.W., Song, I.H., Um, S.H., 2015. Role of physicochemical properties in nanoparticle toxicity. Nanomaterials 5, 1351-1365.

Stark, W.J., 2011. Nanoparticles in biological systems. Angew. Chem. Int. Ed. 50, 1242-1258.

Stefanakis, D., Philippidis, A., Sygellou, L., Filippidis, G., Ghanotakis, D., Anglos, D., 2014. Synthesis of fluorescent carbon dots by a microwave heating process: Structural characterization and cell imaging applications. J. Nanopart. Res. 16.

Suk, J.S., Xu, Q.G., Kim, N., Hanes, J., Ensign, L.M., 2016. PEGylation as a strategy for improving nanoparticle-based drug and gene delivery. Adv. Drug Deliv. Rev. 99, 28-51.

Tian, R.X., Hu, S.L., Wu, L.L., Chang, Q., Yang, J.L., Liu, J., 2014. Tailoring surface groups of carbon quantum dots to improve photoluminescence behaviors. Appl. Surf. Sci. 301, 156-160.

Wang, K., Gao, Z.C., Gao, G., Wo, Y., Wang, Y.X., Shen, G.X., Cui, D.X., 2013. Systematic safety evaluation on photoluminescent carbon dots. Nanoscale Res. Lett. 8, 122.

Wang, L., Wang, X., Bhirde, A., Cao, J., Zeng, Y., Huang, X., Sun, Y., Liu, G., Chen, X., 2014. Carbon dots-based two-photon visible nanocarriers for safe and highly efficient delivery of siRNA and DNA. Adv. Healthcare Mater. 3, 1203-1209.

Wang, Y., Anilkumar, P., Cao, L., Liu, J.H., Luo, P.G., Tackett, K.N., 2nd, Sahu, S., Wang, P., Wang, X., Sun, Y.P., 2011. Carbon dots of different composition and surface functionalization: Cytotoxicity issues relevant to fluorescence cell imaging. Exp. Biol. Med. 236, 1231-1238.

Wörle-Knirsch, J.M., Pulskamp, K., Krug, H.F., 2006. Oops they did it again! Carbon nanotubes hoax scientists in viability assays. Nano Lett. 6, 1261-1268.

Wu, L.L., Li, X.L., Ling, Y.F., Huang, C.S., Jia, N.Q., 2017. Morpholine derivative-functionalized carbon dots-based fluorescent probe for highly selective lysosomal imaging in living cells. ACS Appl. Mater. Interfaces 9, 28222-28232.

Wu, Y.F., Wu, H.C., Kuan, C.H., Lin, C.J., Wang, L.W., Chang, C.W., Wang, T.W., 2016. Multi-functionalized carbon dots as theranostic nanoagent for gene delivery in lung cancer therapy. Sci. Rep. 6, 12.

Xia, J., Chen, S., Zou, G.Y., Yu, Y.L., Wang, J.H., 2018. Synthesis of highly stable red-emissive carbon polymer dots by modulated polymerization: from the mechanism to application in intracellular pH imaging. Nanoscale 10, 22484-22492.

Xie, Y.T., Zheng, J.X., Wang, Y.L., Wan, J.L., Yang, Y.Z., Liu, X.G., Chen, Y.K., 2019. One-step hydrothermal synthesis of fluorescence carbon quantum dots with high product yield and quantum yield. Nanotechnology 30, 10.

Xiong, Y., Schneider, J., Reckmeier, C.J., Huang, H., Kasák, P., Rogach, A.L., 2017. Carbonization conditions influence the emission characteristics and the stability against photobleaching of nitrogen doped carbon dots. Nanoscale 9, 11730-11738.

Xu, X.Y., Ray, R., Gu, Y.L., Ploehn, H.J., Gearheart, L., Raker, K., Scrivens, W.A., 2004. Electrophoretic analysis and purification of fluorescent single-walled carbon nanotube fragments. J. Am. Chem. Soc. 126, 12736-12737.

Yang, S.T., Wang, X., Wang, H.F., Lu, F.S., Luo, P.J.G., Cao, L., Meziani, M.J., Liu, J.H., Liu, Y.F., Chen, M., Huang, Y.P., Sun, Y.P., 2009. Carbon dots as nontoxic and high-performance fluorescence imaging agents. J. Phys. Chem. C 113, 18110-18114.

Yang, X.D., Wang, Y., Shen, X.R., Su, C.Y., Yang, J.H., Piao, M.J., Jia, F., Gao, G.H., Zhang, L., Lin, Q., 2017. One-step synthesis of photoluminescent carbon dots with excitation independent emission for selective bioimaging and gene delivery. J. Colloid Interface Sci. 492, 1-7.

Yuan, Y., Guo, B., Hao, L., Liu, N., Lin, Y., Guo, W., Li, X., Gu, B., 2017. Doxorubicin-loaded environmentally friendly carbon dots as a novel drug delivery system for nucleus targeted cancer therapy. Colloid Surf. B-Biointerfaces 159, 349-359.

Zhang, X., Wang, Y., Liu, W., Liang, X., Si, B., Liu, E., Hu, X., Fan, J., 2017. Facile preparation of surface functional carbon dots and their application in doxorubicin hydrochloride delivery. Mater. Lett. 209, 360-364.

Zuo, P.L., Lu, X.H., Sun, Z.G., Guo, Y.H., He, H., 2016. A review on syntheses, properties, characterization and bioanalytical applications of fluorescent carbon dots. Microchim. Acta 183, 519-542.